Adsorption of Orange G Dye on Hydrophobic Activated Bentonite from Aqueous Solution

Zohra Taibi, Kahina Bentaleb, Zohra Bouberka, Christel Pierlot, Maxence Vandewalle, Christophe Volkringer, Philippe Supiot, Ulrich Maschke

crystals

MDPI

Article

Adsorption of Orange G Dye on Hydrophobic Activated Bentonite from Aqueous Solution

Zohra Taibi [1], Kahina Bentaleb [1], Zohra Bouberka [1,2], Christel Pierlot [3], Maxence Vandewalle [3], Christophe Volkringer [3], Philippe Supiot [1] and Ulrich Maschke [1,*]

[1] Laboratoire Physico-Chimie des Matériaux-Catalyse et Environnement (LPCMCE), Université des Sciences et de la Technologie d'Oran Mohamed Boudiaf (USTOMB), BP 1505, El M'naouer, Oran 31000, Algeria
[2] UMET—Unité Matériaux et Transformations, UMR 8207, Université de Lille, CNRS, INRAE, Centrale Lille, F-59000 Lille, France
[3] Unité de Catalyse et Chimie du Solide (UCCS), UMR 8181, Université de Lille, CNRS, Centrale Lille, F-59000 Lille, France
* Correspondence: ulrich.maschke@univ-lille.fr

Abstract: This report focusses on the modification of physical structure and chemical properties of a bentonite clay from the Hammam Boughrara region of the Maghnia district in western Algeria to maximize its adsorption capacity. The purified bentonite clay (called B) was modified, either by acid activation with 1M sulfuric acid (B-Act), or by intercalation with the cationic surfactant cetytrimethyl ammonium bromide (CTAB), applying a cation exchange capacity (CEC) of 100% (called B-CTAB). Modification of B was also introduced by combining these two steps consecutively, i.e., at first acid activation of B, followed by intercalation with CTAB (B-Act-CTAB). The B-Act-CTAB was obtained by H_2SO_4 (1M) acid activation, followed by co-adsorption of CTAB with 100% and 300% of the CEC of B-Act as precursor. In particular, a strong increase of surface area and pore volume of the modified bentonites was observed for B-Act (469.83 m^2/g and 0.401 cm^3g^{-1}), B-Act-CTAB100 (267.72 m^2/g and 0.316 $cm^3\ g^{-1}$) and B-Act-CTAB300 (111.15 m^2/g and 0.171 cm^3g^{-1}), compared to B (31.79 m^2/g and 0.074 $cm^3\ g^{-1}$) and B-CTAB (3.79 m^2/g and 0.034 $cm^3\ g^{-1}$), respectively. The bentonite-based adsorbents were then used to evaluate the removal efficiency of an organic molecule, the azo dye Orange G (OG), as a model for a Persistent Organic Pollutant. Freundlich, Langmuir and Sips (Langmuir–Freundlich) models were applied to analyze equilibrium isotherms, showing a good correlation between experimental data and the Freundlich model. A good agreement was obtained between experimentally obtained kinetic adsorption data and the pseudo-second-order model, allowing to evaluate rate constants. B-Act-CTAB300 can be applied as a low-cost material for removal of azo dyes, since its adsorption capacity towards OG (102.80 mg/g) exceeds largely that of B-CTAB (31.49 mg/g) and B-Act-CTAB100 (12.77 mg/g).

Keywords: adsorption; activated bentonite; organophilic-activated bentonite; CTAB; Orange G

Citation: Taibi, Z.; Bentaleb, K.; Bouberka, Z.; Pierlot, C.; Vandewalle, M.; Volkringer, C.; Supiot, P.; Maschke, U. Adsorption of Orange G Dye on Hydrophobic Activated Bentonite from Aqueous Solution. *Crystals* **2023**, *13*, 211. https://doi.org/10.3390/cryst13020211

Academic Editor: Robert F. Klie

Received: 10 November 2022
Revised: 19 January 2023
Accepted: 21 January 2023
Published: 24 January 2023

1. Introduction

Over the past years, the use of clays as adsorbents increased rapidly for a wide range of applications. The adsorption capacity of these minerals can be enhanced by modifying their surface properties via thermal [1] and/or chemical processes [2]. One of the most conventional chemical alterations of clay minerals, which is applied for both scientific and commercial targets, is their acid activation, which is achieved by their reaction with a mineral acid solution [3]. In particular, good activation results were obtained by using sulphuric acid. The main objective is to obtain a partially dissolved material of greater specific surface area (SSA), porosity and surface acidity. The first step of acid activation consists of replacing protons by exchangeable cations, and then leaching of metal ions of both tetrahedral and octahedral sites occurs, leaving the remaining silicate groups largely intact [4,5]. Many research groups investigated acid activation of clays [6,7], demonstrating that the

process depends considerably on several elements, such as nature and relative amount of the acid, the treatment time and temperature [8]. Chmielarz et al. [9] reported that the acid nature only weakly influences the properties of the resulting activated adsorbent. Steudel et al. [10] found out that acid activation significantly affects the structural morphology, causing an increase of both SSA and number of active adsorbent sites. These results indicate that dioctahedral clay minerals resist better to acid attack than trioctahedral ones. The delamination of illite occurs slower than for smectites and vermiculites [10]. Longer reaction times of non-swellable clay minerals were observed compared to those of swellable ones of similar composition of the octahedral sheet. Conversely, the amount of acid used has a strong impact on the final properties of the acid-activated clays. Hussin et al. [11] and Santos et al. [12] have investigated the acid activation of various clays. The SSA of these clays was enhanced by increasing the amount of acid, in spite of the significant decrease of the cation exchange capacity (CEC).

An increase of surface area of raw clays by as much as five times was reported by Christidis et al. [13], after hydrochloric acid treatment of bentonite. This increase may be caused by production of finely dispersed silicon oxide from destruction of mineral structures, removal of amorphous Al or silica components, plugging surface pores or interlayer spaces, formation of cracks and voids on the surface [14]. Activated clays are used for a wide range of industrial applications, particularly as adsorbents. In wastewater, activated clay efficiently removes heavy metals, pesticides and other hazardous contaminants [15–17]. Teng–Chien et al. [18] evaluated the adsorption performance of activated bentonite clay particles for the removal of sulfone compounds from oxidized diesel through equilibrium and kinetic studies. The initial sulfur content of 1109.3 ppm was reduced to less than 6 ppm, corresponding to almost 100% removal, using 10 g activated clay, and an agitation of 300 rpm at a temperature of 363 K. Bendaho et al. [19] used activated Algerian clay as an adsorbent to remove Methyl Orange (OM) from aqueous solution. They found fast adsorption during the first 10 min, whereas equilibrium was attained after 30 min.

Similarly, Ullah et al. [20] and Syed et al. [21] investigated the effect of adsorbent dosage, contact time, pH and temperature on the adsorption of Mordant Red 73 (MR73) dye on activated bentonite. Activation was achieved using different organic and inorganic acids, such as phosphoric, acetic, citric and oxalic acids, indicating that activated bentonite could be potentially applied as an adsorbent for textile wastewater treatment. Adsorption of MR73 was found to be temperature- and pH-dependent, and the adsorption equilibrium data followed well the pseudo-second-order kinetic model.

El Mouzdahir et al. [22] investigated the adsorption of Methylene Blue (MB), a basic dye, from aqueous solution, using an activated clay mineral as adsorbent. Improvement of adsorption capacity of the raw clay mineral was achieved by thermal treatment during 2 h at 300 °C, and clay activation using nitric acid (0.5 mol/dm^3), applying reflux conditions. A maximum removal of 500 mg/g of MB at equilibrium was obtained. Experimental equilibrium data were analyzed using Freundlich, Langmuir and Sips (Langmuir–Freundlich) isotherm adsorption models.

However, removal of anionic and hydrophobic pollutants from aqueous media reveals to be unsuccessful for activated clays, since they possess hydrophilic characteristics and are negative charged. The interlayer cations of montmorillonite can be exchanged by surfactant cations [23]. The resulting organoclay presents a significantly enhanced organophilicity and has shown excellent adsorption properties for diverse organic pollutants, e.g., anionic dye [24]. Quaternary alkylammonium compounds (bromides or chlorides) were commonly employed for intercalation into bentonites, such as cetyltrimethyl ammonium bromide (CTAB), the most used compound. Several studies reported about adsorptive characteristics of modified montmorillonite towards organic contaminants [25,26]. Ashna and Heydari [27] showed that CTAB-modified montmorillonite (MMT) can be used to effectively remove Reactive Red. The authors observed that the amount of adsorbed dye onto CTAB-MMT reached its maximum at pH=3. At 60 min of adsorption time, 99.6% of the dye was removed from the solution. Experimental data agreed well with the Langmuir isotherm model. A

maximum adsorption capacity (q_{max}) of 25.8 mg/g was obtained. Ouachtak et al. [28] demonstrated that CTAB-modified bentonite can be also used to effectively remove Orange G (OG) dye from aqueous solution. They observed that the adsorption process did not require pH adjustment, and that optimum adsorption was found in a wide range of pH between 2 and 9. Adsorption isotherm data were best fitted applying the Langmuir model. The maximum adsorption capacity was calculated using the non-linear form of the Langmuir isotherm, resulting 167 mg g/L at 298 K.

This report aims to investigate the adsorption efficiency of a purified low-cost west Algerian natural bentonite clay (called B), as well as that of B-modified, either by acid activation (called B-Act), or by intercalation with CTAB (called B-CTAB). Modification of B will also be introduced by combining these two steps consecutively, i.e., at first acid activation of B, followed by intercalation with CTAB (B-Act-CTAB). As far as we are aware, such a combined approach of acidic activation and organic cationic intercalation of a bentonite clay has not been reported before. The physicochemical properties of B, as well as those of the obtained modified bentonites (B-Act, B-CTAB, and B-Act-CTAB), will be determined applying several characterization techniques. The bentonite-based adsorbents will be used to evaluate the removal efficiency of the anionic OG dye, as model molecule for a Persistent Organic Pollutant.

2. Materials and Methods

2.1. Materials

The bentonite clay was procured from the Hammam Boughrara region of the Maghnia district in western Algeria. Table 1 shows its chemical composition.

The other reagents used were sulfuric acid H_2SO_4 p.a. (Honeywell—Fluka, Seelze, Germany), characterized by a purity of 95–97%, and CTAB ($C_{19}H_{42}NBr$), purchased from Sigma–Aldrich (Steinheim, Germany), with a purity of 99%, exhibiting a molecular weight of 364.45 g/mol and a Critical Micelle Concentration (CMC) of 1 mM in water at room temperature. The organic pollutant used as a model substance was the azo dye OG (99% purity) (see Figure 1), which was obtained from Biochem (Cosne sur Loire, France) and was applied in all adsorption experiments without further purification. OG is very soluble in water, since it contains a sulphonate bond which gives it the anionic character.

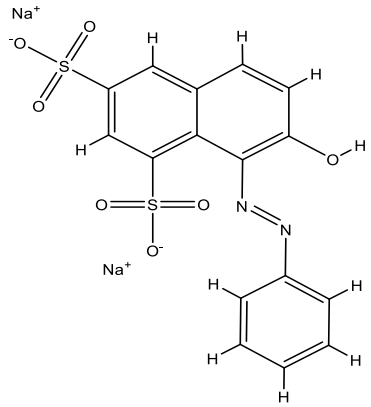

Figure 1. Molecular structure of Orange G (OG) dye.

2.2. Activated Bentonite as Precursor

In a three-necked glass reactor, 5 g of bentonite was mixed with 500 mL of 1 M H_2SO_4 solution. The reactor was partially immersed in an oil bath. Stirring was initiated and the condenser was cooled down to a temperature of 25 °C. The oil bath was then slowly heated to 90 °C and kept at this temperature under reflux condition for 6 h. After cooling down to room temperature, the acid treated powder was separated from solution by centrifugation, washed with deionized water until all traces of acid disappeared, dried for 48 h at 80 °C, and then crushed and sieved. This material will be identified as (B-Act).

2.3. Preparation of CTAB-Modified Activated Bentonite

The preparation of CTAB-modified B-Act, designated as B-Act-CTAB100 and B-Act-CTAB300, was carried out by following the method reported by Bouberka et al. [29]. Accordingly, a defined amount of CTAB was dissolved in distilled water at room temperature, and B-Act precursor (the term "precursor" describes the as synthesized bentonite (activated with H_2SO_4)) was added to the solution. The surfactant was then mixed with bentonite, applying either 100% or 300% of the theoretical CEC = 29.80 meq/100 g of B-Act precursor. The dispersion was shaken for 24 h using a magnetic stirrer. The mixture was then centrifugated and washed with deionized water until no bromide ion could be detected by silver nitrate solution, and later dried at 80 °C for 24 h.

2.4. Characterization of Adsorbents

The value of CEC is determined by the method using complex of copper ethylenediamine [30]. The chemical composition was obtained by fluorescence spectrometry (Philips Magix-Pro, Philips Analytical, Almelo, The Netherlands). The results were reported in mass-% of oxides for the major elements. XRD analysis was done by using Riguka Miniflex 600 X-ray diffractometer (Riguka, Tokyo, Japan) equipped at 40 kV and 15 mA with Cu Kα radiation (λ = 1.5406 Å Goniometer Miniflex 300/600). The samples were scanned from 2° to 80° (2θ) using a step scan of 0.02° and a counting time per step of 0.5 s. Observations of sample morphology were carried out using a Scanning Electron Microscope (SEM) JEOL JSM-7800F (JEOL, Tokyo, Japan), equipped with an energy dispersive spectrometer (EDX) for chemical analysis. The sample as dispersed powder was fixed on a support by means of a double-sided conductive carbon tape. A nanometer-thick chrome layer was deposited to avoid electronic charging. Attenuated Total Reflectance Fourier Transform infrared (ATR-FTIR) spectra were measured in the range 400–4000 cm^{-1} with a resolution of 4.0 cm^{-1} by using a Perkin Elmer Frontier spectrophotometer (PerkinElmer France SAS, Villebon sur Yvette, France). The total surface area (S_{BET}) was quantified by the BET method, while external or non-microporous surface area (S_{EXT}) and the presence of micropores were estimated by the t-plot method. The distribution of the size of the micropores was analyzed according to the methods suggested by Horvath and Kawazoe. The method of Barrett–Joyner–Halenda (BJH) was used to evaluate the average diameter of pores (APD). To identify the effect of modification on the surface charge of the adsorbents, zeta potential measurements were carried out with a Zetasizer Nano ZS (Malvern, Malvern Instruments, England). 1 mg of solid sample was conditioned in 3 mL of aqueous phase, while the ionic strength of the aqueous phase was kept constant at 0.01 M. The pH of the dispersion was adjusted using diluted HCl and NaOH.

2.5. Adsorption Experiments

The adsorption capacities of OG on the adsorbents were investigated by a batch method. UV–Visible spectroscopy was performed using a Double Beam Specord plus 210 UV-Vis spectrophotometer from Analytik-Jena (Jena, Germany), by applying scans from 200 to 800 cm^{-1}. The concentrations of OG were determined at the absorbance corresponding to the maximum wavelength (λ_{max} = 478 nm), and computed from the calibration curves. Two replicates per sample were analyzed and averaged results are presented. The equilibrium concentration of OG, q_e (mg/g), was calculated from the following mass balance (Equation (1)):

$$q_e = \frac{(C_{0-}C_e)}{m} \times V \quad (1)$$

where V represents the volume of the solution (L), C_0 and C_e are initial and equilibrium concentrations of OG (mg/L), respectively, and m stands for the mass of adsorbent (g).

The removal efficiency R (%), corresponding to the percentage of adsorbed OG at equilibrium, was expressed as follows:

$$R\ (\%) = \frac{(C_0 - C_e) \times 100}{C_0} \quad (2)$$

A fixed amount of sample (1 g) was added to 1000 mL of OG solution with an initial concentration of 50 mg/L at 3000 rpm under constant temperature. Samples were collected with a predetermined time schedule (10, 20, 30, 40, 50, 70, 90, 120, 140 and 150 min). In order to investigate the adsorption mechanism, the non-linear form of the pseudo-first-order [31] and the pseudo-second-order [32] kinetic rate equations are given as Equations (3) and (4), respectively:

$$q_t = q_e(1 - e^{-k_1 t}) \quad (3)$$

$$q_e = \frac{k_2 q_2^2}{1 + k_2 q_e t} t \quad (4)$$

where q_t is the adsorbed amount at any time t (mg/g), k_1 stands for the first-order rate constant (1/min), and k_2 is the second-order rate constant (g/mg·min).

The effect of adsorbent dosage was studied using different adsorbent weights from 10 to 50 mg at fixed dye concentration of 50 mg/L. The effect of pH on the amount of dye removal was analyzed over the pH range from 2 to 10, whereby adjustment was made using 0.1 N NaOH and 0.1 N HCl solutions with the same conditions. Isothermal studies were conducted by adding 0.1 g of the clay to 100 mL of dye solution of varying concentration from 10 mg/L to 200 mg/L. The adsorption isotherm results were analyzed using Freundlich [33] (Equation (5)), Langmuir [34] (Equation (6)) and Sips (Langmuir-Freundlich) [35] (Equation (7)) isotherms:

$$q_{e=k_f} C_e^{\left(\frac{1}{n}\right)} \quad (5)$$

$$q_e = \frac{k_L q_m}{1 + K_L C_e} C_e \quad (6)$$

$$q_{e=} \frac{q_{smax} b_s C_e^{\beta}}{1 + b_s C_e^{\beta}} \quad (7)$$

where k_f and $1/n$ are Freundlich constants related to adsorption capacity and adsorption intensity, respectively. q_m represents the monolayer adsorption capacity of the adsorbent, and k_L is the Langmuir constant related to the affinity of the binding sites (L/mg). q_{smax} corresponds to the Sips maximum adsorption capacity (mg/g), b_s represents the equilibrium constant for a heterogeneous solid, and β stands for the heterogeneity parameter.

3. Results and Discussion

3.1. Characterization of Modified Bentonite

3.1.1. Chemical Analysis

The XRF analysis was carried out to determine the chemical composition of the clays and the chemical changes resulting from their modification. The composition of the bentonites before and after modification are presented in Table 1.

Table 1. Chemical composition of Bentonite and all modified Bentonites (B-Act, B-CTAB, B-Act-CTAB100 and B-Act-CTAB300).

Content of Oxides (Weight (w)%)	Bentonite	B-Act	B-CTAB	B-Act-CTAB 100	B-Act-CTAB 300
SiO_2	57.67	79.43	65.77	81.96	77.31
Al_2O_3	18.72	12.04	15.45	11.43	11.55
MgO	9.60	4.60	6.60	4.10	4.00
Fe_2O_3	3.62	1.71	7.15	1.52	1.59
CaO	0.39		0.17		
K_2O	0.88	0.78	1.41	0.69	0.77
Na_2O	7.40				
SO_3	0.18	0.84			0.64
Br			2.90		3.66
TiO_2	0.09	0.13	0.15	0.13	0.15
SiO_2/Al_2O_3	3.08	6.59	4.25	7.16	6.69
$SiO_2/(Al_2O_3 + MgO + Fe_2O_3)$	1.80	4.32	2.25	4.80	4.51

The chemical analysis of bentonite revealed that SiO_2 and Al_2O_3 represent the major elements. Si and Al are often associated with structures of clay, quartz and feldspars, whereas Na_2O, Fe_2O_3 and MgO are only present in small amounts. All other oxides such as CaO, K_2O and TiO_2 are present in trace amounts. The apparition of TiO_2 can be explained by the presence of impurities in the clay sample. The ratio SiO_2/Al_2O_3 was calculated as 3.08, superior than 2, indicating that the bentonite was of montmorillonite nature. The Na_2O, CaO and K_2O contents of the bentonite show that these elements are located in the interlayer. The chemical composition of the clay allows to calculate the subsequent chemical formula: $(Si_{6.45},Al_{1.23})(Mg_{1.6},Fe_{0.15})$ $(Na_{0.8},Ca_{0.04},K_{0.06},Ti_{0.007})$.

After modification, the bentonite composition changed considerably. Indeed, modification of bentonite (B-Act, B-CTAB, B-Act-CTAB100 and B-Act-CTAB300) provokes decreasing contents of MgO, CaO, Na_2O, Fe_2O_3 and Al_2O_3 while SiO_2 content increased. The reduction of octahedral cations, as well as the increase of Si^{4+}, leads to an increase of the ratio of SiO_2 to the sum of the other metal oxides ($SiO_2/\sum M_xO_y$) from 1.80 to 4.32–4.80. Si^{4+} tetrahedral cations may be less leached by acid attack than Al^{3+} octahedral cations [36]. The Bentonite mineral shows a gradual decrease of CEC from 101.03 to (29.8~1.11) meq/100 g (Table 2). A breakdown of the bentonite structure was found during HCl modification [37], provoking a precipitation of hydrous silica phases. Octahedrally coordinated Mg, Fe and Al were released into the solution, completing thus the decomposition of the clay structure.

Table 2. Summary of data for the d_{001} reflexion (basal spacing), cation exchange capacity (CEC), and S_{BET} for all samples analyzed.

Clay Sample	Basal Spacing (Å)	S_{BET} (m^2/g)	CEC (meq/100 g)
Bentonite	12.72	32.79	101.03
B-Act	15.30	469.83	29.80
B-CTAB	20.93	3.79	n.d
B-Act-CTAB100	14.95	267.72	1.11
B-Act-CTAB300	17.58	111.15	22.04

A clear reduction of the sodium portion was observed, since the Na_2O composition of bentonite is 7.40, and for modified clays no value was detected. Therefore it may be concluded that Na^{2+} represents a major exchangeable cation. The decreasing amount of Na^{2+} and Ca^{+2} ions (in weight% of Na_2O, CaO) for B-Act, B-Act-CTAB100 and B-Act-CTAB300 may be explained by a replacement by monovalent hydrogen ion during the activation process, and for B-CTAB, it means probably that the amount of alkylammonium cations are intercalated into the basal space of bentonite. Evidence of these findings are supported by the XRD results.

When comparing SiO_2/Al_2O_3 ratios for B-Act, B-Act-CTAB100 and B-Act-CTAB300, it was found that B-Act-CTAB100 and B-Act-CTAB300 possess greater ratios than B-Act, due to the loss of Al_2O_3 (Table 1). This can be related to larger mean particle sizes of B-Act-CTAB100 and B-Act-CTAB300, evidenced by BET analysis. The following chemical formula can be proposed for B-Act: $(Si_{8.89}, Al_{0.79})(Mg_{0.76}, Fe_{0.07})(K_{0.05}, Ti_{0.01})$, for B-Act-CTAB100: $(Si_{9.18}, Al_{0.75})(Mg_{0.68}, Fe_{0.06})(K_{0.04}, Ti_{0.01})$ and for B-Act-CTAB300: $(Si_{8.66}, Al_{0.76})$ $(Mg_{0.\ 66}, Fe_{0.06})$ $(K_{0.05}, Ti_{0.012})$.

3.1.2. Cation Exchange Capacity (CEC)

The values of CEC were calculated for bentonite, B-CTAB, B-Act, B-Act-CTAB100 and B-Act-CTAB300, yielding 101.03, n.d, 29.80, 1.11, and 22.04 meq/100g, respectively (Table 2).

The decrease of CEC of the modified bentonites (B-Act, B-CTAB, B-Act-CTAB100, B-Act-CTAB300) compared to bentonite is due to activation by H_2SO_4 and loading with CTAB surfactant. Some exchangeable cations were replaced during the activation by H^+ from sulfuric acid and by CTA^+ from cetyltrimethyl ammonium. In order to balance the negatively charged clay surfaces, the latter attract exchangeable positive ions contained in the solutions [38]. The CEC was reduced by pH treatment [39], and elements can also be released from the octahedral sheet [40].

3.1.3. XRD Analysis

The powder X-ray diffraction patterns of modified bentonite (B-CTAB and B-Act) compared to initial bentonite are presented in Figure 2a, which were found to be typical for layered structures. Structural changes in the samples can be seen mainly in the intensity and height of the d_{001} reflection of bentonite. The diffraction pattern of bentonite exhibited a crystal line structure with an intense reflection at $2\theta = 6.94°$ ([001] reflection) with $d_{001} = 12.72$ Å characteristic of montmorillonite, at $2\theta = 19.98°$ ([100] reflection) with $d_{100} = 4.44$ Å; $2\theta = 28.69°$ ([114] reflection) with $d_{114} = 3.109$ Å, and two others at $2\theta = 35.18°$ and 61.92° corresponding at $d_{105} = 2.54$ Å and $d_{300} = 1.49$ Å, respectively (JCPDS 13-0135). The peaks with (2θ) values of 14.475 (6.11 Å) [001] and 28.05 (3.18 Å) correspond, respectively, to [112] planes, indicating the presence of kaolinite (JCPDF 05-0221). Quartz (SiO_2) represents the dominant impurity in montmorillonite and kaolinite minerals, at $2\theta = 26.76°$ ([101] reflection) with $d_{022} = 3.33$ (JCPDS 87-2096) with other lines at $2\theta = 35.18°$ with $d_{002} = 2.54$ Å for cristobalite (SiO_2), $2\theta = 43.50$ for albite ($AlNaO_8Si_3$) and at $2\theta = 28.69°$ for calcite.

Such findings imply that the bentonite mineral contains mainly montmorillonite with two layers of water in the interlayer space [41], mixed with small amounts of kaolinite, quartz, and minor albite and calcite amounts. The major reflection of d_{001} of bentonite, depicted at 6.94°, is the most important reflection used for monitoring the success of modification.

B-CTAB showed a shift of d_{001} reflection towards lower angles, indicating the increase of d_{001} from 12.72 Å to 20.93 Å (Table 2), representing the successful intercalation of the surfactant between the layers. First, adsorption of CTAB occurs by cation exchange on the external surface and into the interlayer space. Subsequently, the CTAB adsorption proceeds via van der Waals interactions. The double- or triple-layer arrangement of CTAB leads to an extension of basal spacing in montmorillonite to 18 Å and 25 Å, respectively [42]. Indeed, an increase from $d_{001} = 12.72$ Å to 20.93 Å was already found for B-CTAB.

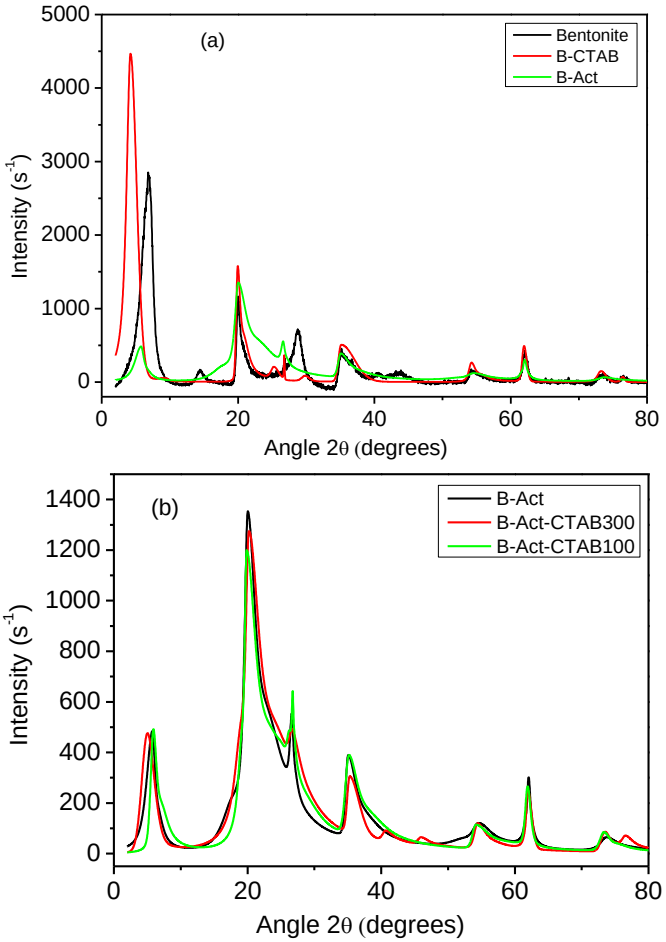

Figure 2. XRD patterns of (**a**) Bentonite, B-CTAB and B-Act; (**b**) B-Act and organo-acid-activated bentonite with different CTAB loadings corresponding to 100% and 300% CEC (B-Act-CTAB100 and B-Act-CTAB300), respectively.

For the activated clay sample (B-Act), the characteristic peak of kaolinite at d = 6.11 Å disappears, and the two reflections at 12.72 (2θ = 6.94°) and 3.33 Å (2θ = 26.76°) correspond respectively to montmorillonite. On the other hand, a decrease in intensity was observed which can be related to an alteration in the internal clay structure during the activation process: the crystalline phase content of montmorillonite decreased, but there was an evidence of increase of the interlayer distance. A similar trend was observed by Bijang et al. [43]. The X-ray peak positions and intensities observed for B-Act, B-Act-CTAB100, and B-Act-CTAB300 (Figure 2b) are nearly the same: B-Act and B-Act-CTAB 100 present similar basal spacing (B-Act: d_{001} = 15.30 Å, and B-Act-CTAB100: d_{001} = 14.95 Å), indicating that CTAB surfactant at 100% CEC does not provoke significant modification in the basal spacing. Such coating of the activated bentonite can drastically change mineral properties by decreasing CEC (Table 2). Indeed, CEC decreases from 29.80 to 1.11 meq/100 g. The intercalation of surfactants at 300% CEC into the interlayer space of the clay mineral (B-Act-CTAB300) resulted in a shift of the d_{001} peak position in the direction of lower values of 2θ. B-Act-CTAB300 presents a basal spacing of 17.58 Å at 2θ = 5.02°, whereas B-Act shows a basal spacing of 15.30 Å at 2θ = 5.76°. Considering that the length of the CTAB surfactant molecule is approximately 25 Å, it appears that, in this case, the surfactants formed a monolayer in the interlayer space of the clay.

This study focused on the interactions between a bentonite previously activated with acid H_2SO_4 (1M) and the long-chain molecule CTAB. For B-CTAB, the material was prepared from the initial swelling bentonite; it is for this reason that the surfactant could be intercalated inside the reticular distance and increasing thus this distance. For B-Act-CTAB,

the material was prepared from acid-activated bentonite which was not swelling and was partially deteriorated; therefore, the surfactant could not intercalate and just reacted with the external surface.

3.1.4. Analysis by Scanning Electron Microscopy

SEM micrographs of bentonite and B-Act are shown in Figure 3, and present a pronounced difference in their corresponding architectures. Indeed, the surface morphology of bentonite (Figure 3a) reveals to be different from that of B-Act (Figure 3b).

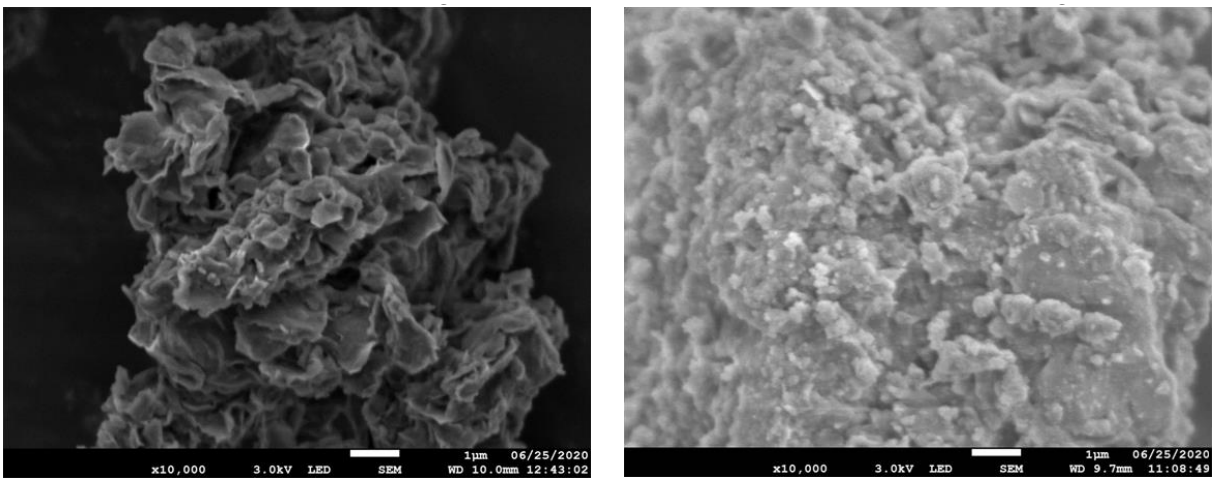

(**a**) (**b**)

Figure 3. Microscopic analysis of clay materials by SEM: (**a**) bentonite; (**b**) B-Act.

The H_2SO_4 treatment partially altered the morphological structure of bentonite, which will be clarified hereinafter. The bentonite sample showed larger particle aggregates with smooth surfaces, but after H_2SO_4 activation, the porous structure was improved (Figure 3b). The acid allocation into the interior of bentonite was followed by the substitution of ions, forming a dense collection of the acid-activated clay. The SEM image of B-Act reveals that the microstructure was formed by a relatively homogeneous and compact clay matrix; it also shows the parallel layout of the leaves clayey. As will be shown in Section 3.1.5, a decrease in the size of B-Act particles was observed, as well as an increase in the apparent porosity of the B-Act surface, compared to bentonite.

3.1.5. N_2 Adsorption/Desorption

Nitrogen adsorption–desorption isotherms of B-Act-CTAB100 and B-Act-CTAB300, as well as for B-Act, B-CTAB and B-Na+, are shown in Figure 4, and the textural parameters are gathered in Table 3. As shown in Figure 4, all isotherms exhibit type IVa with a hysteresis loop of type H3, corresponding to the IUPAC (International Union of Pure and Applied Chemistry) classification [44,45], which is characteristic for a mesoporous structure.

The physisorption isotherms of type IVa are related to a capillary condensation occurring in the mesopores, reducing the absorption on a wide range of P/P_0. Type IVa isotherms imply also multilayered sorption. The inflection points of the isotherms are not well defined, indicating that in the beginning, the formation of mono- and multilayers occurred on the surface of the adsorbent [46]. A H3 hysteresis loop corresponds to a solid consisting of agglomerate particles with a small amount of micropores with non-uniform size or shape of slit-shaped pores [47]. The specific surface area of the bentonite used in this work (S_{BET} = 32.79 m^2 g^{-1}) is lower than that of other bentonite clays: S_{BET} = 35.70 m^2 g^{-1} (Jelšovy Potok (Slovakia); Andrunik et al. [48]); S_{BET} = 77m^2 g^{-1} (North-east of Morocco; Ouachtak et al. [28]); S_{BET} = 66.2 $m^2.g^{-1}$ (Al Azraq (Jordan); Khansaa Al-Essa [49]). This variation of S_{BET} represents a specific feature of clay which can differ from one clay to another and is subject to its origin. The specific surface areas and total pore volumes are

S_{BET} = 469.83 m^2 g^{-1} (0.401 cm^3 g^{-1}), 267.72 m^2 g^{-1} (0.316 cm^3 g^{-1}) and 111.15 m^2 g^{-1} (0.171 cm^3 g^{-1}) for B-Act, B-Act-CTAB100, and B-Act-CTAB300, respectively. An increase of surface area and total pore volume is observed for all modified clays, compared to the pristine bentonite.

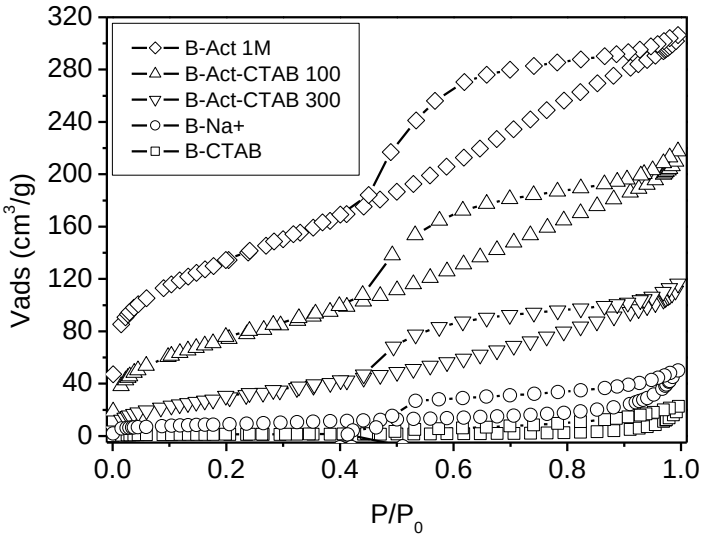

Figure 4. N_2 adsorption-desorption isotherms of bentonite and all modified bentonites.

Table 3. Specific surface area (S_{BET}), external surface area (S_{EXT}) and micropore volume ($V_{\mu P}$) of bentonite and all modified bentonite clays. S_{tot}: Total surface area derived from the slope of the straight line passing through the origin of the t-plot. $V_{\mu P}$: Liquid micropore volume derived from the ordinate at the origin in the second straight line of the t-plot. $S_{\mu pt}$ micro: Surface area out of micropores derived from the slope of the second straight line of the t-plot. V_{tot}: Total pore volume (TPV), derived from the amount of nitrogen adsorbed at $P = P_0 = 0.995$.

Samples	$S_{(BET)}$ ($m^2.g^{-1}$)	$S_{Langmuir}$ ($m^2.g^{-1}$)	S_{tot} ($m^2.g^{-1}$)	S_{ext} ($m^2.g^{-1}$)	V_{tot} TPV ($cm^3.g^{-1}$)	$V_{\mu P}$ ($cm^3.g^{-1}$)	$S_{\mu P}$ ($m^2.g^{-1}$)	APD (nm)
Bentonite	32.8	45.3	18.6	28.4	0.074	0.001	3.4	12.7
B-CTAB	3.8	5.7	2.5	2.1	0.034	0.0008	1.8	39.9
B-Act	469.8	669.6	271.3	409.3	0.401	0.028	60.5	4.6
B-Act-CTAB100	267.7	385.9	147.7	279.5	0.316	−0.008	nd	5.3
B-Act-CTAB300	111.2	163.9	59.9	140.3	0.171	−0.016	nd	5.8

After acid activation, an enhancement of textural properties of the bentonite was observed as a consequence of replacement of K^+, Na^+ and Ca^{2+} (exchangeable cations) with H^+ ions, and removing impurities, and could be attributed to splitting of clay particles within the dissolved octahedral which expose the edges of the plates [50]. The high surface area of modified bentonite (viz., B-Act, B-Act-CTAB100 and B-Act-CTAB300) is attributed to the reduction of the pore size (APD) of the particles (Table 3), due to the removal of adsorbed water and formation of meso- and micropores. B-Act displayed the largest surface area out of micropores ($S_{\mu p}$), induced by the formation of additional microporous volume. Co-adsorption of CTAB on B-Act decreased the microporous surface (nd). However, the BET analysis demonstrate a lower surface area and pore volume for B-CTAB (3.754 m^2 g^{-1} (0.034 cm^3 g^{-1})), explained by the fact that the interlayer space of bentonite, which is occupied by the CTAB cations, is not easily accessible to N_2 molecules [51]. The calculated external surface areas (S_{ext}) and total pore volume V_{tot} (TPV) using the Barrett–Joyner–Halenda (BJH) method are also given in Table 3. In the case of B-Act, B-Act-CTAB100

and B-Act-CTAB300, the values of S_{ext} are higher than S_{BET}, which may indicate that the surface is located in a wider pore fraction. However, in the case of bentonite and B-CTAB, S_{ext} is lower than S_{BET}, which may indicate that the surface is mostly located in narrower pore fraction.

Figure 5 presents the pore size distribution curves (dV/dr versus r) for B, B-Act, B-CTAB, B-Act-CTAB100 and B-Act-CTAB300. The pore size distributions of B-Act, B-Act-CTAB100 and B-Act-CTAB300 show one peak dominating in the mesoporous range, which was not shown for B and B-CTAB. It is evident that B and B-CTAB predominantly have micropores with mean radii of less than 2 nm. Moreover, the pore size distribution curve of B-Act-CTAB300 indicates a bimodal system with a bigger fraction of wider pores than the other clays. The peak maximum of B-Act at 3.85 nm is shifted to 3.79 nm for B-Act-CTAB100 and to 3.48 nm for B-Act-CTAB300, indicating a narrow pore size distribution, when CTAB is co-adsorbed.

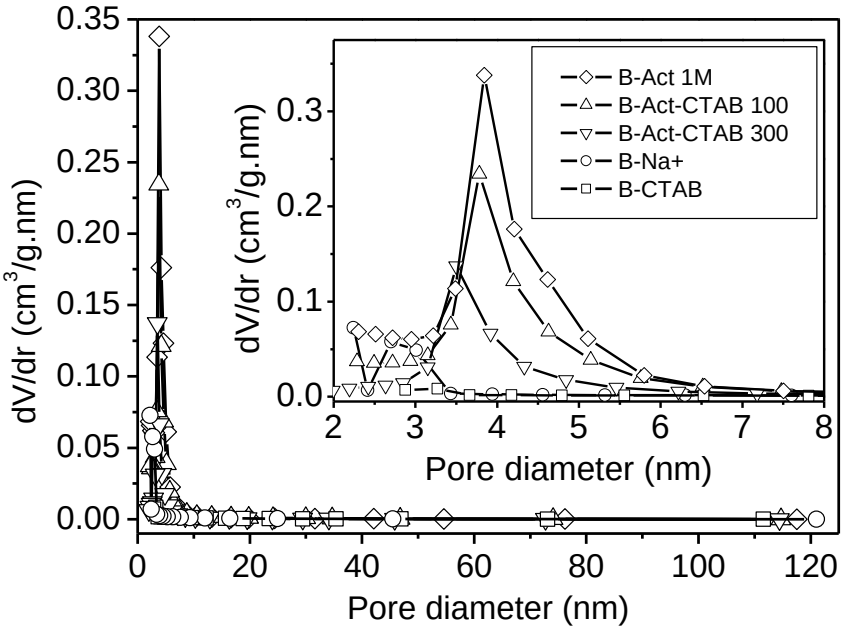

Figure 5. Pore Size Distribution (PSD) models of studied clay samples.

3.1.6. Infrared Spectroscopy Analysis

Distinct changes can be observed when comparing the FTIR spectrum of B-Act with that of bentonite (Figure 6a). The most significant change is a decrease of the intensity of the bands at 3620 cm^{-1} and 997 cm^{-1} of B-Act assigned to the stretching vibration of the hydroxyl groups coordinated to octahedral Al^{3+} cations (Al-OH-Al, along with the Al-Mg-OH). The intensity of these bands is reduced compared to the spectrum of bentonite, and can be attributed to the release of octahedral cations from the structure (confirmed by chemical analysis, Table 1). Intense bands at around 3406 cm^{-1} and 1623 cm^{-1} from bentonite can be assigned to O-H stretching and bending vibration of HO-H for the water molecule of hydration. Changes occur involving these bands after acid attack, i.e., these bands (3406 cm^{-1} and 1623 cm^{-1}) vanished, due to the partial dissolution of the main bentonite structure. The protons from acid activation penetrate into the clay layers attacking the OH groups, causing the alteration of adsorption bands (OH- and octahedral cations). In particular, the band at 1623 cm^{-1} disappeared for B-Act, owing to the loss of adsorbed water as function of temperature and time applied to activate bentonite.

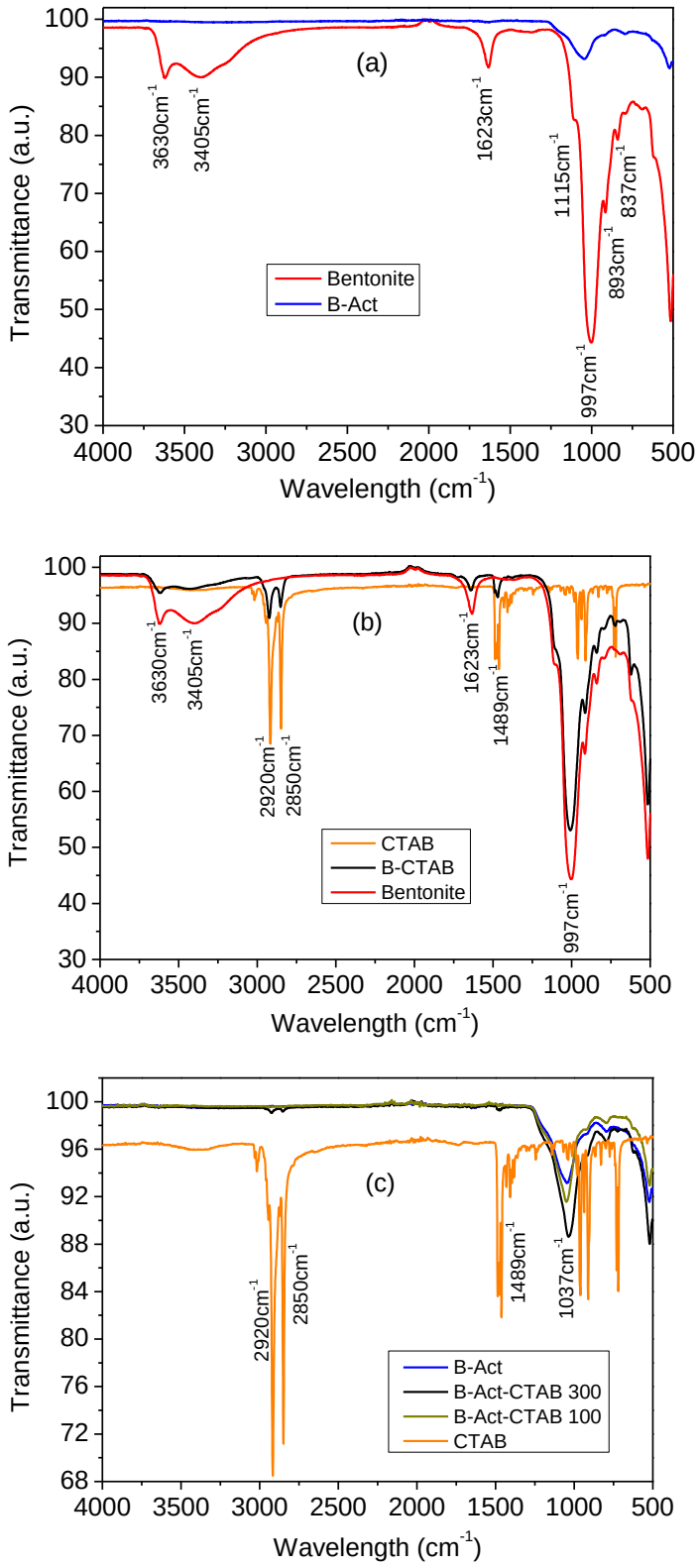

Figure 6. FTIR spectra of (**a**) Bentonite and B-Act, (**b**) Bentonite, CTAB and B-CTAB, and (**c**) B-Act, CTAB, B-Act-CTAB100 and B-Act-CTAB300.

Comparable results for activated bentonite were reported in literature [7]. Acid activation of clays represents a two-step procedure in which the splitting of particles within the octahedral sheet occurs. At first, the exchange cations are replaced by protons. Then, leaching of octahedral cations takes place, such as Al^{3+}, Mg^{2+} and Fe^{3+}, from octahedral

and tetrahedral sheets [52]. The frequency of the band at 997 cm^{-1}, corresponding to the deformation vibrations of Si-O, shifts, and its intensity decreases. Bending vibrations of Si–O-Mg (461 cm^{-1}), Si-O-Al (517 cm^{-1}) and Si-O (797 cm^{-1}) can be related to the partial dissolution of aluminum ions present in the octahedral sheet of bentonite.

The spectrum of B-CTAB (Figure 6b) shows new adsorption bands at 2850 cm^{-1} and 2920 cm^{-1}, corresponding to symmetric and anti-symmetric stretching vibrations modes of $–CH_2$ and $–CH_3$ groups of the aliphatic chain of CTAB, respectively [25,53]. Moreover, an absorption peak appears at 1489 cm^{-1}, which can be associated to an ammonium ion [46].

The appearance of these bands confirms the organophilization of the clay, since they can be regarded as attached to CTAB in free or bound positions of the bentonite.

Figure 6c presents the FTIR spectra of B-Act, CTAB, B-Act-CTAB100 and B-Act-CTAB300. The spectrum of B-Act-CTAB100 did not present any new bands compared to B-Act, suggesting that this method cannot detect the small quantity of CTAB co-adsorbed by this sample. The effectiveness of the modification of B-Act with CTAB at 300% CEC is confirmed by the presence of weak absorption bands in the range 2922–2851 cm^{-1}, which represent methylene groups (CH_2) and at 1489 cm^{-1}, together with the main bands in the B-Act spectrum.

3.1.7. Zeta Potential

Figure 7 presents the pH effect on the zeta potential of bentonite, B-CTAB, B-Act, B-Act-CTAB100 and B-Act-CTAB300. The isoelectric point (pH_{iep}) is a pH value at which the total amount of positive charge on the surface of the solid is equal to the total amount of negative charge on it. The amount of net surface charge of solid or zeta potential value is zero at the isoelectric point. For any pH < pH_{iep}, the clay develops a positive charge. It becomes a favorable material for the adsorption of anionic species, such as OG.

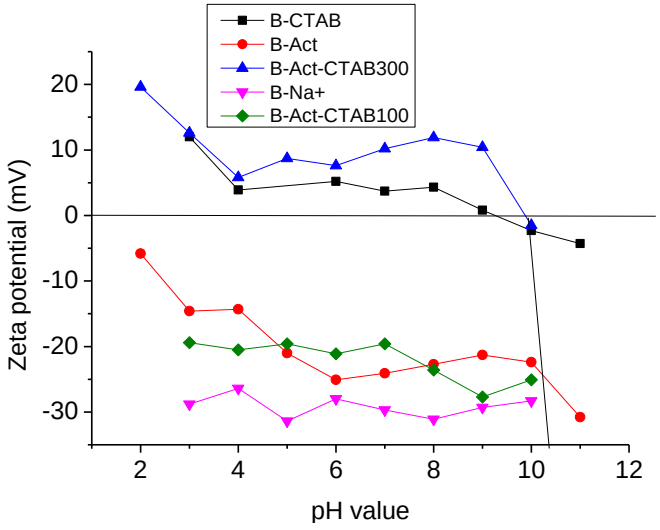

Figure 7. Zeta potential as function of pH of bentonite compared to all synthesized samples.

The isoelectric point can be determined by the intersection of the zeta potential as a function of pH, with the x-axis at zeta potential equal to zero. The zeta potential of the studied dispersions shows distinct values between (B-CTAB and B-Act-CTAB300) on one side, and (bentonite, B-Act and B-Act-CTAB100) on the other side. In the range from pH = 2 to 11, the latter ones remain negatively charged for all pH values. An increase of pH provokes an increase of the negative charge. These samples did not show an isoelectric point because isomorphic substitution remains independent of pH in the acidic range. Under basic conditions, the edge surface of bentonite and B-Act, where the octahedral/tetrahedral sheet is broken, can be assimilated with the surface of alumina or silica particles [54]. The hydroxyl ion acts like an ion, determining the Zeta potential, and provokes a negative charge of the surface of the edge [55].

Figure 7 reveals also that CTAB introduced an important positive charge on bentonite. The surface of B-CTAB and B-Act-CTAB300 are composed of positive sites, representing mainly CTA^+ ions. The point of zero charge of B-CTAB and B-Act-CTAB300 was found at approximately pH_{iep} = 9. Indeed, the zeta potential value was about 0.8mV at pH = 9 for B-CTAB, and 0.87mV at pH = 9.7 for B-Act-CTAB300. The clay surface changes from hydrophilic to hydrophobic and from negative to positive charge, when the cationic surfactant CTAB is adsorbed into the interlayer spacing and onto the external surface of the clay. B-Act-CTAB100 sample shows negative zeta potential values, indicating that an amount of 100% CEC reveals to be not sufficient to neutralize completely the negative surface charge of B-Act.

3.2. Adsorption of Orange G Dye

3.2.1. Effect of Contact Time

Removal efficiency of bentonite and B-Act towards OG dye remains lower than 2% in the range of concentrations studied, and could be considerably enhanced when modification occurs by surfactant. The kinetics of adsorption were considered to compare the adsorption rates of B-CTAB, B-Act-CTAB100 and B-Act-CTAB300. The influence of contact time on removal of OG dye (50 mg/L) at pH = 6 and 20 °C is shown in Figure 8 and summarized in Table 4. It is evident that all samples successfully adsorb OG dye with different efficiencies. The dye adsorption of B-Act-CTAB300 is faster than that of both B-CTAB and B-Act-CTAB100. Moreover, the maximum amount of adsorbed dye (q_e) is higher for B-Act-CTAB300 (52.40 mg/g) than for B-CTAB (28.14 mg/g) and B-Act-CTAB100 (6.32 mg/g). To reach equilibrium, it takes 50 and 80 min for B-Act-CTAB300 and B-CTAB, and 30 min in the case of B-Act-CTAB100. The surface charge and the degree of ionization of adsorbate are mainly responsible for the removal of the dye from aqueous solution. The amount of adsorption increases with increasing heterogeneity of the structure.

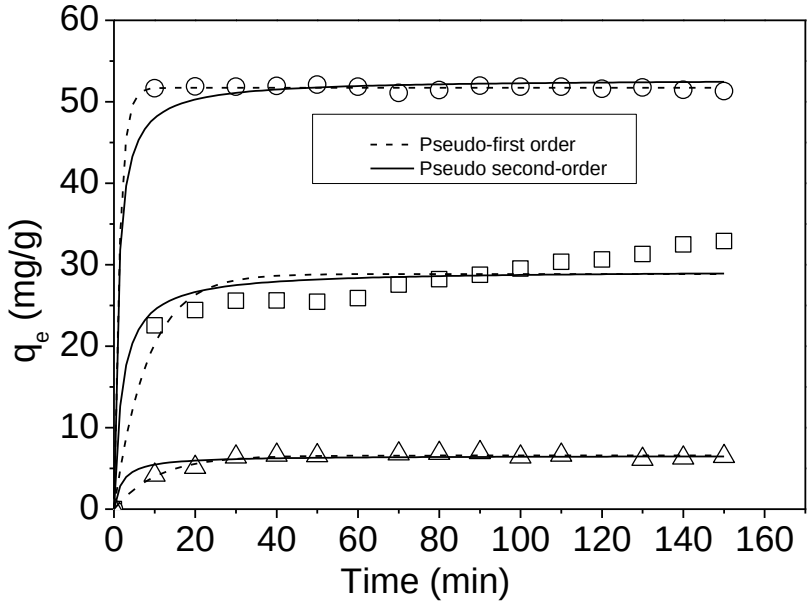

Figure 8. Adsorption kinetics: effect of contact time of removal of OG dye by (o) B-Act-CTAB300, (□) B-CTAB and (Δ) B-Act-CTAB100. Conditions: dye concentration 50 mg/L; adsorbent dosage m_s = 1 g/L; pH = 6; T = 298 ± 1 K. Continuous and dashed lines correspond to fits of the experimental data.

Table 4. Kinetic constants for pseudo-first- and pseudo-second-order models for OG dye adsorption on B-CTAB, B-Act-CTAB100 and B-Act-CTAB300.

Adsorbents	q_e (exp) (mg/g)	Pseudo-First-Order Model			Pseudo-Second-Order Model		
		k_1 (min^{-1})	q_e (cal) (mg/g)	R^2	k_2 (g/mg min)	q_e (cal) (mg/g)	R^2
B-CTAB	28.94	0.120	28.86	0.892	0.0170	29.31	0.916
B-Act-CTAB300	52.40	0.699	51.71	0.999	0.0189	52.79	0.991
B-Act-CTAB100	6.32	0.093	6.58	0.976	0.0762	6.55	0.980

Interestingly, B-Act-CTAB100 with negative zeta potential still adsorbs the anionic dye, although the latter should be repelled electrostatically from the negatively charged surface. Indeed, loading by co-adsorption of CTAB on B-Act increases the affinity of B-Act-CTAB100 with regard to OG. The surface properties of B-Act-CTAB100 and B-Act-CTAB300 change from hydrophilic to hydrophobic character and lead, therefore, to an increasing adsorption capacity towards anionic dyes.

B-CTAB possesses a very interesting basal spacing, favoring the adsorption phenomenon. However, once these were occupied, the remaining vacant surface sites became increasingly difficult to be occupied by OG. The dye molecules were adsorbed into the interlayer space, due to the high d_{001} value, followed by an interaction between the negatively charged sulphonate groups of the dye and the cationic surfactant head groups of high positive charge.

The experimental data were fitted by using pseudo-first-order and pseudo-second-order kinetic models, considering an initial OG dye concentration of 50 mg/L. The rate constants k_1, k_2 and q_e (cal), obtained from plots applying Equations (2) and (3), and q_e (exp) from Figure 8, together with correlation coefficients R_1 and R_2, are gathered in Table 4.

As result, the kinetic data of B-CTAB, B-Act-CTAB100 and B-Act-CTAB300 followed the pseudo-second-order model with high correlation coefficient (R^2) values of 0.916 for B-CTAB, 0.991 for B-Act-CTAB300 and 0.980 for B-Act-CTAB100, whereas the pseudo-first-order model yielded R^2 values of 0.892, 0.999 and 0.976, respectively. The q_e (exp) values (28.94 mg/g for B-CTAB, 52.40 mg/g for B-Act-CTAB300 and 6.32 mg/g for B-Act-CTAB100) were in close agreement with q_e (cal) (29.31 mg/g for B-CTAB; 52.79 mg/g for B-Act-CTAB300 and 6.55 mg/g for B-Act-CTAB300 for the pseudo-second-order model. From the consideration of the adsorbent dye interactions, the pseudo-second-order model seems to be more suitable than the pseudo-first-order model. Adsorption kinetics of dyes on clay follow generally the pseudo-second-order model [56–58]. From literature, it is known that physical adsorption can be described by the pseudo-first-order kinetic model, whereas the pseudo-second-order kinetic model can be applied to fit chemical adsorption phenomena [59,60]. Indeed, OG molecules are likely to hold two adsorption sites, instead of only one, on solid surfaces [61]. As a consequence, B–Act-CTAB300 presents faster kinetics and higher adsorption capacity than the other adsorbents. This signifies a stronger reaction between OG and some active sites of the same activity in contrast with other sites on the B–Act-CTAB300 surface. The possibility of intraparticle diffusion resistance affecting adsorption process could be explored using the intraparticle diffusion model.

3.2.2. Effect of Initial Dye Concentration

The relationship between the amount of dye, adsorbed per unit mass of adsorbent and its equilibrium concentration in solution is presented in Figure 9, in order to estimate the interaction between adsorbate and adsorbents. Figure 9 shows a non-linear evolution of the adsorption isotherms with curvatures concave to the abscissa. The quantity of adsorbed OG dye increases at low adsorbate concentration, indicating that adsorption sites are available in excess, and saturation was reached progressively with increasing adsorbate concentration. The lowest OG dye removal was obtained using B-Act-CTAB100 as adsorbent. More important dye quantities were adsorbed by B-CTAB and B-Act-CTAB300, respectively. In the

range of concentrations comprised between 10 and 200 mg/L, B-CTAB and B-Act-CTAB300 remove 15.74 and 51.40%, respectively. The adsorption capacity of B-Act-CTAB100 is lower than that of B-Act-CTAB300, due to their different hydrophobicities, since the surface of B-Act-CTAB300 clay is not important. Thus, Orange G was essentially adsorbed onto the organo-activated bentonite via hydrophobic and organophilic interactions.

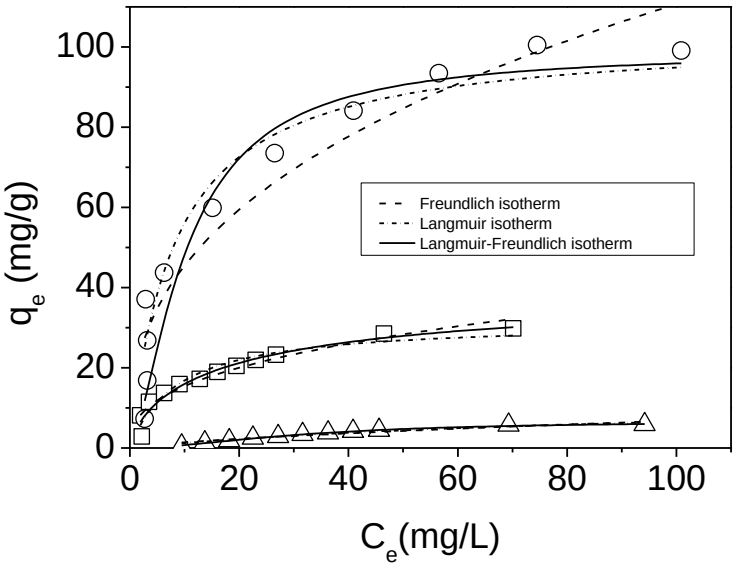

Figure 9. Adsorption isotherms of dye removal on (o) B-Act-CTAB300, (□) B-CTAB and (Δ) B-Act-CTAB100 samples. Conditions: dye concentration C_0 = 10 to 200 mgL^{-1}; adsorbent dosage m_s = 1 g/L; pH = 6; T = 298 ± 1 K.

The experimental adsorption data of OG dye were analyzed by the non-linear form of the Langmuir, Freundlich and Langmuir–Freundlich (Sips) models, in order to get better understanding of the possible adsorption mechanism. The obtained parameters from these isotherms were gathered in Table 5. As a result, Langmuir isotherms fit the experimental data very well for B-CTAB, B-Act-CTAB100 and B-Act-CTAB300, with high R^2 and low RMSE (Root Mean Square Error) values. Moreover, a good agreement was found between corresponding values of calculated maximum adsorption capacity (q_{max}) of the Langmuir model and the experimental data, confirming that this model describes well the dye adsorption process.

Table 5. Langmuir, Freundlich and Sips isotherm model parameters for OG dye adsorption onto B-CTAB, B-Act-CTAB100 and B-Act-CTAB300.

Isotherms	**Parameters**	**Adsorbents**		
		B-CTAB	B-Act-CTAB100	B-Act-CTAB300
Langmuir	$q_{L,max}$ (mg/g)	31.5	12.8	102.8
	b_L *(L/mg)*	0.12	0.011	0.12
	R^2	0.944	0.958	0.940
	RMSE	3.5	0.12	72.97
Freundlich	k_f $(mg/g)^{1-1/n}$	6.45	0.30	18.67
	1/n	0.38	0.68	0.39
	R^2	0.927	0.912	0.906
	RMSE	4.55	0.26	108.1
Sips (L-F)	q_{Smax} (mg/g)	29.8	6.8	103.7
	b_S *(L/mg)*	0.12	0.0018	0.1
	β	1.05	1.82	1.05
	R^2	0.930	0.996	0.946
	RMSE	4.41	0.013	62.8

The Langmuir model considers that the surface is homogeneous, so that adsorption of OG onto modified bentonite can be regarded as a monolayer adsorption without interaction between the adsorbed molecules, since adsorbent and adsorbate strongly interact [62]. In Table 6, q_{max} data taken from literature were put together with the data from this report. To compare these data, one should take into consideration variations of experimental conditions of some sources. It can be concluded that B-Act-CTAB300 exhibits significantly higher adsorption capacity of OG, in contrast with the other cited adsorbents.

Table 6. Comparison of adsorption capacity of B-CTAB, B-Act-CTAB100 and B-Act-CTAB300 with other published data.

Adsorbent	q_{max} (mg/g)	Adsorbent Dosage (g/L)	Reference
Activated carbon of Thespesia populnea pods	9.129	8	[63]
γ- alumina nanoparticles	93.3	1	[64]
Formaldehyde modified Ragi husk	14.6	2	[65]
Raw Chitin	15.42	10	[66]
Polystyrene-modified Chitin	17.86	10	[66]
Magnetic graphene oxide nanocomposite	20.85	1	[67]
B-CTAB	31.49	1	Present work
B-Act-CTAB100	12.77	1	Present work
B-Act-CTAB300	102.80	1	Present work

3.2.3. Effect of Initial pH

The dye-adsorbent interaction depends essentially on their structures. The pH of a solution affects the degree of ionization and speciation of dyes, which are complex organic compounds with different functional groups and unsaturated bonds. Blank studies for OG dye were undertaken in the pH range comprised from 2 to 12. After the pH adjustment, the dye solutions were kept for 1 h; then, the absorbance of the solutions was determined. Changing the pH value did not change significantly the absorbance spectra of the dye. On the other hand, protonation and deprotonation of functional groups on the surface vary the chemical structure of clays [68,69]. The pH_{zpc} values were found as 9.2 and 10.5 for B-CTAB and B-Act-CTAB300, respectively (see Figure 7). At pH < pH_{zpc}, the surface charge of adsorbents was positive, while it became negative when pH > pH_{zpc}. The B-Act-CTAB100 sample presents negative zeta potential values in the whole range of pH values (see Figure 7), indicating a reduction of the density of ionizable OH groups during the previous treatment. However, this density is still high enough to maintain the surface negatively charged, as mentioned by Whitby et al. [70].

Figure 10 represents the percentage of adsorbed OG from solutions exhibiting different pH values. Adsorption of OG remains at a high level for B-Act-CTAB300 when the pH was varied between 2 and 10. In this range, 95% dye removal was recorded, using 50 mg/L as initial dye concentration. Thus, B-Act-CTAB300 bears a positive charge on its surface in the pH range 2–10, which confirms the high OG dye removal by electrostatic attraction forces, occurring between positively charged clay surface sites and the anionic dye. A sharp decrease from 95% to 65% of the OG adsorption appeared for pH values exceeding 10, which might be attributed to repulsion effects between negatively charged B-Act-CTAB 300 clay particles and anionic dye molecules [71].

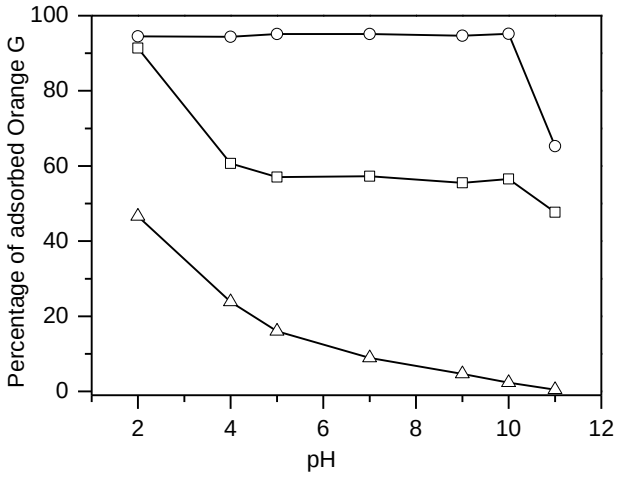

Figure 10. Effect of pH on the percentage of adsorbed OG dye on (o) B-Act-CTAB300, (□) B-CTAB and (Δ) B-Act-CTAB100 samples (experimental conditions: C_o = 50 mg/L; m_s = 1 g/L; contact time t = 60 min; T = 298 ± 1 K).

The maximum adsorption on B-CTAB (92%) was observed under acidic conditions (pH = 2). At low pH, electrostatic attractions increase between negatively charged dye anions and positively charged adsorption sites, leading to higher dye adsorption. The percentage of adsorbed OG dye decreased to 60% when the pH increased to 4, and remained more or less stable for higher pH values up to 10. The same type of interaction is thus present between pH = 4 and pH = 10. Above the latter value, a slight decrease was remarked, which might be due to a competition between dye anions and OH- groups for the positive charged sites on B-CTAB adsorbent [72]. The anionic OG dye molecule tends to be adsorbed more efficiently onto B-Act-CTAB300 and B-CTAB via electrostatic attraction between the positively charged head (CTA+) and the negatively charged dye ($-SO_3^-$) (i.e., presence of hydrophobic interaction between anionic dye and alkyl chains of CTAB). The presence of surfactant alkyl chains leads to surface hydrophobicity of B-Act-CTAB300 and B-CTAB.

The removal percentage declined considerably with increasing pH for B-Act-CTAB100, and no removal was recorded at pH = 11. The negatively charged OG dye might be electrostatically repelled by parts of B-Act–CTAB100 surface not covered by CTAB surfactant. The negative charge of the surface raises up when the pH value increases, explaining the growing repulsion between adsorbent and adsorbate. Indeed, a negatively charged surface of B-Act-CTAB100 was found (see Figure 7) for pH values from 2 to 11. Van der Waals- and π–π-interactions become dominant since at pH = 2, the adsorption capacity of OG dye on B-Act-CTAB100 was more important than that for other pH values [73].

4. Conclusions

Bentonite has been successfully activated by sulfuric acid treatment, as shown by FTIR and XRD studies, in addition to an increase of its surface area. The organo-activated bentonites (B-Act-CTAB100 and B-Act-CTAB300) were obtained by organophilization of the activated bentonite (B-Act), using CTAB as a surfactant. These materials were characterized by a series of analysis (XRF, XRD, FTIR, SEM and BET), in order to observe the development of the structural and textural properties after alteration.

The modified bentonites were examined for their adsorption properties of the anionic dye OG. All results showed that B-Act-CTAB300 is a better effective adsorbent for OG than B-Act-CTAB100, B-CTAB and B-Act. The maximum adsorption capacities for OG on B-Act-CTAB300, B-Act-CTAB100 and B-CTAB were determined at 298 K as 102.80, 12.77 and 31.49 mg dye/g adsorbent, respectively. A good agreement of the experimental adsorption data with the Langmuir model was found.

The suitability of kinetic models for dye adsorption on modified bentonites was also discussed. The adsorption kinetics of the dye obeyed pseudo-second-order adsorption kinetics. The adsorption of OG dye onto adsorbents reveals to be a pH-dependent process with maximum removal efficiency in acidic media. Optimization of B-Act-CTAB300 with distinctive adsorption parameters leads to an excellent adsorbent for binding OG molecules.

Author Contributions: Conceptualization, Z.B. and U.M.; methodology, Z.T., Z.B. and U.M.; investigation, Z.T., K.B., M.V. and C.V.; formal analysis, Z.T. and Z.B.; data curation, Z.T., Z.B., C.P., C.V., P.S. and U.M.; writing-original draft preparation, Z.B. and U.M.; writing-review and editing, U.M.; visualization, Z.B. and U.M.; supervision, Z.B. and U.M.; project administration, Z.B. and U.M. All authors have read and agreed to the published version of the manuscript.

Funding: This research received no external funding.

Data Availability Statement: Data are contained within the article.

Acknowledgments: This work is the result of close collaboration between the two laboratories LPCMCE of USTOMB and UMET of the University of Lille, as part of an ERASMUS Plus MIC project (2018–2021), as well as a Hubert Curien Tassili (PHC) research program entitled 18MDU104 (2018–2021). Our thanks therefore go first of all to the various actors who participated in the implementation of these projects. The authors gratefully acknowledge the support of the Algerian Ministry of Higher Education and Scientific Research (MESRS), the General Directorate of Scientific Research and Technological Development (DGRSDT) of Algeria, the University of Sciences and Technology of Oran (USTOMB)/Algeria, the French Ministry of Higher Education and Research (MENESR), the CNRS, and the University and the CROUS of Lille/France.

Conflicts of Interest: The authors declare no conflict of interest.

References

1. Padilla-Ortega, E.; Medellin-Castillo, N.; Robledo-Cabrera, A. Comparative study of the effect of structural arrangement of clays in the thermal activation: Evaluation of their adsorption capacity to remove Cd(II). *J. Environ. Chem. Eng.* **2020**, *8*, 103850. [CrossRef]
2. Arias Espana, V.A.; Sarkar, B.; Biswas, B.; Rusmin, R.; Naidu, R. Environmental applications of thermally modified and acid activated clay minerals: Current status of the art. *Environ. Technol. Innov.* **2019**, *13*, 383–397. [CrossRef]
3. Komadel, P. Chemically modified smectites. *Clay Miner.* **2003**, *38*, 127–138. [CrossRef]
4. Falaras, P.; Kovanis, I.; Lezou, F.; Seiragakis, G. Cottonseed oil bleaching by acid activated montmorillomite. *Clay Miner.* **1999**, *34*, 221–232. [CrossRef]
5. Tsakiri, D.; Douni, I.; Taxiarchou, M. Structural and surface modification of oxalic-acid-activated bentonites in various acid concentrations for bleaching earth synthesis—A comparative study. *Minerals* **2022**, *12*, 764. [CrossRef]
6. Ajemba, R.O. Modification of Ntezi bentonite structure by hydrochloric acid: Process kinetics and structural properties of the modified samples. *Pak. J. Sci. Ind. Res. A Phys. Sci.* **2014**, *57*, 1–9. [CrossRef]
7. Ajemba, R.O. Structural alteration of bentonite from nkaliki by acid treatment: Studies of the kinetics and properties of the modified samples. *Int. J. Adv. Eng. Technol.* **2014**, *7*, 379–392. [CrossRef]
8. Aliu, M.; Pula-Beqiri, L.; Kadriu, S.; Sadiku, M.; Lajçi, N.; Kelmendi, M. Research of the chemical composition and ion exchange properties of Karaçeva bentonite. *J. Int. Environ. Appl. Sci.* **2016**, *11*, 409–413.
9. Chmielarz, L.; Wojciechowska, M.; Rutkowska, M.; Adamski, A.; Węgrzyn, A.; Kowalczyk, A.; Dudek, B.; Boroń, P.; Michalik, M.; Matusiewicz, A. Acid-activated vermiculites as catalysts of the DeNOx process. *Catal. Today* **2012**, *191*, 25–31. [CrossRef]
10. Steudel, A.; Batenburg, L.F.; Fischer, H.R.; Weidler, P.G.; Emmerich, K. Alteration of non-swelling clay minerals and magadiite by acid activation. *Appl. Clay Sci.* **2009**, *44*, 95–104. [CrossRef]
11. Hussin, F.; Aroua, M.K.; Daud, W.M.A.W. Textural characteristics, surface chemistry and activation of bleaching earth: A review. *Chem. Eng. J.* **2011**, *170*, 90–106. [CrossRef]
12. Santos, S.S.G.; Silva, H.R.M.; de Souza, A.G.; Alves, A.P.M.; da Silva Filho, E.C.; Fonseca, M.G. Acid-leached mixed vermiculites obtained by treatment with nitric acid. *Appl. Clay Sci.* **2015**, *104*, 286–294. [CrossRef]
13. Christidis, G.E.; Scott, P.W.; Dunham, A.C. Acid activation and bleaching capacity of bentonites from the islands of Milos and Chios, Aegean, Greece. *Appl. Clay Sci.* **1997**, *12*, 329–347. [CrossRef]
14. Jozefaciuk, G. Effect of acid and alkali treatments on surface-charge properties of selected minerals. *Clays Clay Miner.* **2002**, *50*, 647–656. [CrossRef]
15. Boroomand, N.; Shokria, Z. Adsorption of Cadmium (II) and Copper (II) onto magnetic organo-Bentonite modified by 2-(3,4-Dihydroxyphenyl)-1, 3-Dithiolane from aqueous solutions. *Int. J. Environ. Sci. Dev.* **2017**, *8*, 88–92. [CrossRef]

16. Tha-in, S.; Dau, H.A.; Dumri, K. The enhanced carbamate adsorption of modified bentonite with Coscinium Fenestratum. *Int. J. Environ. Sci. Dev.* **2013**, *4*, 415–418. [CrossRef]
17. Te, B.; Wichitsathian, B.; Yossapol, C. Modification of natural common clays as low cost adsorbents for Arsenate adsorption. *Int. J. Environ. Sci. Dev.* **2015**, *6*, 799–804. [CrossRef]
18. Chen, T.C.; Fe, J.; Sapitan, F.; Ballesteros, F.C.; Lu, M.-C. Using activated clay for adsorption of sulfone compounds in diesel. *J. Clean. Prod.* **2016**, *124*, 378–382. [CrossRef]
19. Bendaho, D.; Driss, T.A.; Bassou, D. Adsorption of acid dye onto activated Algerian clay. *Bull. Chem. Soc. Ethiop.* **2017**, *31*, 51–62. [CrossRef]
20. Ullah, Z.; Hussain, S.; Gul, S.; Khan, S.; Bangash, F.K. Use of HCl-modified bentonite clay for the adsorption of Acid Blue 129 from aqueous solutions. *Desalin. Water Treat.* **2015**, *57*, 8894–8903. [CrossRef]
21. Syed, H.J.; Zahir, A.; Khan, A.; Afzal, S.; Mansha, M. Adsorption of Mordant Red 73 dye on acid activated bentonite: Kinetics and thermodynamic study. *J. Mol. Liq.* **2018**, *254*, 398–405. [CrossRef]
22. El Mouzdahir, Y.; Elmchaouri, A.; Mahboub, R.; Gil, A.; Korili, S.A. Equilibrium modeling for the adsorption of Methylene Blue from aqueous solutions on activated clay minerals. *Desalination* **2010**, *250*, 335–338. [CrossRef]
23. Khenifi, A.; Bouberka, Z.; Sekrane, F.; Kameche, M.; Derriche, Z. Adsorption study of an industrial dye by an organic clay. *Adsorption* **2007**, *13*, 149–158. [CrossRef]
24. Manzotti de Souza, F.; Machi Lazarin, A.; Gurgel, M.; Vieira, A.; dos Santos, O.A.A. Kinetic, equilibrium, and thermodynamic study on Atrazine adsorption in organophilic clay. *Desalin. Water Treat.* **2018**, *123*, 240–252. [CrossRef]
25. Chu, Y.; Khan, M.A.; Zhu, S.; Xia, M.; Lei, W.; Wang, F.; Xu, Y. Microstructural modification of organo-montmorillonite with Gemini surfactant containing four ammonium cations: Molecular dynamics (MD) simulations and adsorption capacity for copper ions. *J. Chem. Technol. Biotechnol.* **2019**, *94*, 3585–3594. [CrossRef]
26. Zhao, Q.; Burns, S.E. Modeling sorption and diffusion of organic sorbate in hexadecyltrimethylammonium-modified clay nanopores—A molecular dynamics simulation study. *Environ. Sci. Technol.* **2013**, *47*, 2769–2776. [CrossRef]
27. Ashna, P.; Heydari, R. Removal of Reactive Red 198 from aqueous solutions using modified clay: Optimization, kinetic and isotherm. *J. Chil. Chem. Soc.* **2020**, *65*, 4958–4961. [CrossRef]
28. Ouachtak, H.; El Guerdaoui, A.; Haounati, R.; Akhouairi, S.; El Haouti, R.; Hafid, N.; Ait Addi, A.; Šljukić, B.; Santos, D.M.F.; Labd Taha, M. Highly efficient and fast batch adsorption of orange G dye from polluted water using superb organo-montmorillonite: Experimental study and molecular dynamics investigation. *J. Mol. Liq.* **2021**, *335*, 116560. [CrossRef]
29. Bouberka, Z.; Khenifi, A.; Ait Mahamed, H.; Haddou, B.; Belkaid, N.; Bettahar, N.; Derriche, Z. Adsorption of Supranol Yellow 4 GL from aqueous solution by surfactant-treated aluminum/chromium-intercalated bentonite. *J. Hazard. Mater.* **2009**, *162*, 378–385. [CrossRef]
30. Bergaya, F.; Vayer, M. CEC of clays: Measurement by adsorption of a copper ethylenediamine complex. *Appl. Clay Sci.* **1997**, *12*, 275–280. [CrossRef]
31. Lagergren, S. Zur Theorie der sogenannten Adsorption geloster Stoffe. *Kungliga svenska vetenskapsakademiens Handlingar* **1898**, *24*, 1–39.
32. Ho, Y.-S.; McKay, G. Sorption of dye from aqueous solution by peat. *Chem. Eng. J.* **1998**, *70*, 115–124. [CrossRef]
33. Freundlich, H.M.F. Über die Adsorption in Lösungen. *Z. Phys. Chem.* **1906**, *57*, 385–470. [CrossRef]
34. Langmuir, I. The constitution and fundamental properties of solids and liquids. Part, I. solids. *J. Am. Chem. Soc.* **1916**, *38*, 2221–2295. [CrossRef]
35. Jeppu, G.P.; Clement, T.P. A modified Langmuir–Freundlich isotherm model for simulating pH-dependent adsorption effects. *J. Contam. Hydrol.* **2012**, *129–130*, 46–53. [CrossRef]
36. Mele, A.; Taraj, K.; Korpa, A. Acid activation of Prrenjas clay mineral. *J. Eng. Process. Manag.* **2015**, *7*, 37–44. [CrossRef]
37. Gates, W.P.; Anderson, J.S.; Raven, M.D.; Churchman, G.J. Mineralogy of a bentonite from Miles, Queensland, Australia and characterisation of its acid activation products. *Appl. Clay Sci.* **2002**, *20*, 189–197. [CrossRef]
38. Hattab, A.; Bagane, M.; Chlendi, M. Characterization of Tataouine's raw and activated clay. *J. Chem. Eng. Process. Technol.* **2013**, *4*, 155. [CrossRef]
39. Önal, M. Swelling and cation exchange capacity relationship for the samples obtained from a bentonite by acid activations and heat treatments. *Appl. Clay Sci.* **2007**, *37*, 74–80. [CrossRef]
40. Volzone, C.; Cesio, A.M. Thermal behaviour of Titanium in host matrix clay. *Mat. Res.* **2009**, *12*, 191–196. [CrossRef]
41. Calarge, L.M.; Meunier, A.; Formoso, M.L.L. A bentonite bed in the Aceguà (RS, Brazil) and Melo (Uruguay) areas: A highly crystallized montmorillonite. *J. S. Am. Earth Sci.* **2003**, *16*, 187–198. [CrossRef]
42. Betega de Paiva, L.; Morales, A.R.; Valenzuela Díaz, F.R. Organoclays: Properties, preparation and applications. *Appl. Clay Sci.* **2008**, *42*, 8–24. [CrossRef]
43. Bijang, C.; Wahab, A.W.; Maming; Ahmad, A.; Taba, P. Design of Bentonite acid modified electrodes in cyanide biosensors. *Int. J. Mater. Sci Appl.* **2015**, *4*, 115–119. [CrossRef]
44. Broekhoff, J.C.P. Mesopore determination from nitrogen sorption isotherms: Fundamentals, scope, limitations. *Stud. Surf. Sci. Catal.* **1979**, *3*, 663–684. [CrossRef]
45. Shields, J.E.; Lowell, S.; Thomas, M.A.; Thommes, M. *Characterization of Porous Solids and Powders: Surface Area, Pore Size and Density*; Kluwer Academic Publisher: Boston, MA, USA, 2004; pp. 43–45.

46. Thommes, M.; Kaneko, K.; Neimark, A.V.; Olivier, J.P.; Rodriguez-Reinoso, F.; Rouquerol, J.; Sing, K.S.W. Physisorption of gases, with special reference to the evaluation of surface area and pore size distribution (IUPAC Technical Report). *Pure Appl. Chem.* **2015**, *87*, 1051–1069. [CrossRef]
47. Touaa, N.D.; Bouberka, Z.; Gherdaoui, C.; Supiot, P.; Roussel, P.; Pierlot, C.; Maschke, U. Titanium and iron-modified delaminated muscovite as photocatalyst for enhanced degradation of Tetrabromobisphenol A by visible light. *Funct. Mater. Lett.* **2020**, *13*, 2051008. [CrossRef]
48. Andrunik, M.; Bajda, T. Modification of Bentonite with cationic and nonionic surfactants: Structural and textural features. *Materials* **2019**, *12*, 3772. [CrossRef]
49. Al-Essa, K. Activation of Jordanian Bentonite by hydrochloric acid and its potential for olive mill wastewater enhanced treatment. *J. Chem.* **2018**, 8385692. [CrossRef]
50. Valenzuela Díaz, F.R.; De Souza, S.P. Studies on the acid activation of Brazilian smectitic clays. *Quim. Nova* **2001**, *24*, 345–353. [CrossRef]
51. Haounati, R.; Ouachtak, H.; El Haouti, R.; Akhouairi, S.; Largo, F.; Akbal, F.; Benlhachemi, A.; Jada, A.; Addi, A.A. Elaboration and properties of a new SDS/ CTAB@Montmorillonite organoclay composite as a superb adsorbent for the removal of malachite green from aqueous solutions. *Sep. Purif. Technol.* **2021**, *255*, 117335. [CrossRef]
52. Ajemba, R. Enhancement of physicochemical properties of NteJe clay to increase its bleaching performance using acid activation. *Int. J. Eng. Res. Appl. (IJERA)* **2012**, *2*, 281–288.
53. Fil, B.A.; Yilmaz, M.T.; Bayar, S.; Elkoca, M.T. Investigation of adsorption Astrazon Red Violet 3RN (Basic Violet 16) dyestuff onto Montmorillonite Clay. *Braz. J. Chem. Eng.* **2014**, *31*, 171–182. [CrossRef]
54. Xu, L.; Wu, H.; Dong, F.; Wang, L.; Wang, Z.; Xiao, J. Flotation and adsorption of mixed cationic/anionic collectors on muscovite mica. *Miner. Eng.* **2013**, *41*, 41–45. [CrossRef]
55. Daud, N.K.; Hameed, B.H. Decolorization of Acid Red 1 by Fenton-like process using rice husk ash-based catalyst. *J. Hazard. Mater.* **2010**, *176*, 938–944. [CrossRef]
56. Benguella, B.; Yacouta-Nour, A. Elimination des colorants acides en solution aqueuse par la Bentonite et le Kaolin. *C. R. Chim.* **2009**, *12*, 762–771. [CrossRef]
57. Bhakta, J.N.; Munekage, Y. Identification of potential soil adsorbent for the removal of hazardous metals from aqueous phase. *Int. J. Environ. Sci. Technol.* **2013**, *10*, 315–324. [CrossRef]
58. Ozcan, A.S.; Ozcan, A. Adsorption of acid dyes from aqueous solutions onto acid-activated bentonite. *J. Colloid Interface Sci.* **2004**, *276*, 39–46. [CrossRef]
59. Wang, L.; Wang, A. Adsorption properties of congo red from aqueous solution onto surfactant-modified montmorillonite. *J. Hazard. Mater.* **2008**, *160*, 173–180. [CrossRef]
60. Vimonses, V.; Lei, S.; Jin, B.; Chow, C.W.K.; Saint, C. Kinetic study and equilibrium isotherm analysis of congo red adsorption by clay materials. *Chem. Eng. J.* **2009**, *148*, 354–364. [CrossRef]
61. Zaker, Y.; Hossain, M.A.; Islam, T.S.A. Adsorption kinetics of methylene blue onto clay fractionated from Bijoypur soil, Bangladesh. *Res. J. Chem. Sci.* **2013**, *3*, 65–72.
62. Rusmin, R.; Sarkar, B.; Liu, Y.; McClure, S.; Naidu, R. Structural evolution of chitosan-palygorskite composites and removal of aqueous lead by composite beads. *Appl. Surf. Sci.* **2015**, *353*, 363–375. [CrossRef]
63. Arulkumar, M.; Sathishkumar, P.; Palvannan, T. Optimization of Orange G dye adsorption by activated carbon of Thespesia populnea pods using response surface methodology. *J. Hazard. Mater.* **2011**, *186*, 827–834. [CrossRef] [PubMed]
64. Banerjee, S.; Dubey, S.; Gautam, R.V.; Chattopadhyaya, M.C.; Sharma, Y.C. Adsorption characteristics of alumina nanoparticles for the removal of hazardous dye, Orange G from aqueous solutions. *Arab. J. Chem.* **2019**, *12*, 5339–5354. [CrossRef]
65. Dev, V.V.; Wilson, B.; Nair, K.K.; Antony, S.; Anoop Krishnan, K. Response surface modeling of Orange G adsorption onto surface tuned ragi husk. *Colloids Interface Sci. Commun.* **2021**, *41*, 100363. [CrossRef]
66. Umar, A.; Sanagi, M.M.; Abu Naim, A.; Wan Ibrahim, W.N.; Abdul Keyon, A.S.; Wan Ibrahim, W.A. Removal of Orange G from aqueous solutions by Polystyrene-modified Chitin. *J. Teknol. (Sci. Eng.)* **2017**, *79*, 91–99. [CrossRef]
67. Deng, J.-H.; Zhang, X.-R.; Zeng, G.-M.; Gong, J.-L.; Niu, Q.-Y.; Liang, J. Simultaneous removal of Cd (II) and ionic dyes from aqueous solution using magnetic graphene oxide nanocomposite as an adsorbent. *Chem. Eng. J.* **2013**, *226*, 189–200. [CrossRef]
68. Largo, F.; Haounati, R.; Akhouairi, S.; Ouachtak, H.; El Haouti, R.; El Guerdaoui, A.; Hafid, N.; Santos, D.M.F.; Akbal, F.; Kuleyin, A.; et al. Adsorptive removal of both cationic and anionic dyes by using sepiolite clay mineral as adsorbent: Experimental and molecular dynamic simulation studies. *J. Mol. Liq.* **2020**, *318*, 114247. [CrossRef]
69. Ouachtak, H.; Akhouairi, S.; Addi, A.A.; Akbour, R.A.; Jada, A.; Douch, J.; Hamdani, M. Mobility and retention of phenolic acids through a goethite-coated quartz sand column. *Colloids Surf. A Physicochem. Eng. Asp.* **2018**, *546*, 9–19. [CrossRef]
70. Whitby, C.P.; Scales, P.J.; Grieser, F.; Healy, T.W.; Nishimura, S.; Tateyama, H. The adsorption of dodecyltrimethylammonium bromide on mica in aqueous solution studied by X-ray diffraction and atomic force microscopy. *J. Colloid Interface Sci.* **2001**, *235*, 350–357. [CrossRef]
71. Abidi, N.; Duplay, J.; Jada, A.; Errais, E.; Ghazi, M.; Semhi, K.; Trabelsi-Ayadi, M. Removal of anionic dye from textile industries effluents by using Tunisian clays as adsorbents. Zeta potential and streaming-induced potential measurements. *C. R. Chim.* **2019**, *22*, 113–125. [CrossRef]

72. Mall, I.D.; Srivastava, V.C.; Agarwal, N.K. Removal of Orange-G and Methyl Violet dyes by adsorption onto bagasse fly ash—Kinetic study and equilibrium isotherm analyses. *Dyes Pigm.* **2006**, *69*, 210–223. [CrossRef]
73. Chinoune, K.; Bentaleb, K.; Bouberka, Z.; Nadim, A.; Maschke, U. Adsorption of reactive dyes from aqueous solution by dirty bentonite. *Appl. Clay Sci.* **2016**, *123*, 64–75. [CrossRef]